

# Computational methods for 2D materials modelling

A. Carvalho<sup>†</sup>

*Centre for Advanced 2D Materials, National University of Singapore, 6 Science Drive 2, 117546 Singapore\* and  
Fondazione Bruno Kessler, Via Sommarive, 18, 38123 Povo TN, Trento, Italy*

P. E. Trevisanutto<sup>†</sup>

*European Centre for Theoretical Studies in Nuclear Physics and Related Areas (ECT\*-FBK)  
and Trento Institute for Fundamental Physics and Applications (TIFPA-INFN),  
Via Sommarive, 14, 38123 Povo TN, Trento, Italy*

S. Taioli<sup>†</sup>

*European Centre for Theoretical Studies in Nuclear Physics and Related Areas (ECT\*-FBK)  
and Trento Institute for Fundamental Physics and Applications (TIFPA-INFN),  
Via Sommarive, 14, 38123 Povo TN, Trento, Italy and  
Peter the Great St. Petersburg Polytechnic University,  
Polytechnicheskaya 29, St. Petersburg 195251, Russia*

A. H. Castro Neto

*Centre for Advanced 2D Materials, National University of Singapore, 6 Science Drive 2, 117546 Singapore\* and  
Materials Science and Engineering, National University of Singapore, 9 Engineering Drive 1, Singapore 117575*

Materials with thickness ranging from a few nanometers to a single atomic layer present unprecedented opportunities to investigate new phases of matter constrained to the two-dimensional plane. Particle-particle Coulomb interaction is dramatically affected and shaped by the dimensionality reduction, driving well-established solid state theoretical approaches to their limit of applicability. Methodological developments in theoretical modelling and computational algorithms, in close interaction with experiments, led to the discovery of the extraordinary properties of two-dimensional materials, such as high carrier mobility, Dirac cone dispersion and bright exciton luminescence, and inspired new device design paradigms. This review aims to describe the computational techniques used to simulate and predict the optical, electronic and mechanical properties of two-dimensional materials, and to interpret experimental observations. In particular, we discuss in detail the particular challenges arising in the simulation of two-dimensional constrained fermions, and we offer our perspective on the future directions in this field. **[Note: for a version with third-party figures, please contact the authors]**

## I. INTRODUCTION

The behaviour of quantum particles, either bosons or fermions, is affected by the dimensionality of the space accessible to them. Developments in nanotechnology and nanofabrication over the last few years made it possible to use dimensionality as a parameter, which can be harnessed by precise control of the atomic structure. In particular, the fabrication of two-dimensional (2D) materials – materials where electrons, phonons or other particles are constrained to a 2D manifold – have revealed a plethora of new phenomena that significantly enriched our knowledge in condensed matter physics. Starting from the synthesis of graphene, the epitome of 2D materials, several novel layered crystal families, such as metallic and semiconducting dichalcogenides, silicene, germanene, and phosphorene, have been discovered. These findings are a potentially disruptive innovation in optoelectronics,

spintronics, electromechanics, energy storage, and thermoelectrics.

To investigate the properties of these novel 2D materials, which are dramatically modified by the reduced screening and quantum confinement, numerical simulations based on first principles, multiscale and more recently machine learning [1, 2] approaches represent an essential tool to interpret and guide experiments. 2D materials can be sub-nanometer thick and may have only a few atoms per unit cell, making it possible to model them with great precision. In fact, surfaces and interfaces are atomically sharp and can be represented accurately by atomistic models. Nevertheless, the coexistence of atomic and solid state features of these 2D architectures have pushed the existing theories to their limits and created a quest for new computational modelling strategies to assess accurately and efficiently both ground and excited state properties.

This manuscript thus reviews (addressing, in particular, the experimental reader) state-of-the-art computational methods used to model 2D materials at different levels of theory. We discuss the theoretical foundations of the numerical methods used to characterise ground and

---

\*Electronic address: carvalho@nus.edu.sg

[†] These authors contributed equally to this work

excited-state properties of 2D materials, their respective range of applicability, and we show a few illustrative examples of the computation of electronic, optical, transport and mechanical properties. Finally, we reflect upon future challenges and directions of this rapidly evolving field.

The article is structured as follows: in section II, we shortly review density functional theory (DFT) for the electronic ground state; in section III, we outline computational approaches based on many-body perturbation theory (MBPT) for electronic excited states; in section IV, we discuss several methods to carry out charge transport simulations; and finally section V is devoted to computational approaches for the simulation of mechanical properties of 2D materials.

## II. DENSITY FUNCTIONAL THEORY

DFT is one of the most used computational methods in materials research and 2D materials in particular. It is implemented in numerous codes and has achieved a high level of reproducibility.[3]. We will briefly introduce the fundamentals of DFT and discuss some of the achievements and challenges in 2D and layered materials.

### A. Fundamentals

DFT is rooted on the two Hohenberg–Kohn theorems [4]. It is an exact formalism, based on a variational principle, that allows one to find the energy and electron density  $n(\mathbf{r})$  of the ground state  $|\Psi\rangle$  of a quantum system. This is conceptually attractive because, unlike the wavefunction, the charge density is an observable. However, in practice, the determination of the electron density of real systems relies on approximations to describe the exchange and correlation interactions between electrons[5]. In particular, the exchange interaction, whereby many-body systems must be antisymmetric under exchange, stems from Pauli’s exclusion principle and acts upon electrons with the same spins. The latter force leads e.g. to spin alignment in ferromagnets or to the Hund’s rule in atoms.

The remainder of the Coulomb interaction after including static exchange, is the electron-electron correlation [5, 6]. The effect of this potential becomes visible e.g. in the dissociation of the  $\text{H}_2$  molecule, where it is responsible for the electrons ending up on different atoms upon *adiabatic* bond stretching [7]. We notice that in the context of DFT, the correlation energy is defined differently from other fields of computational chemistry and condensed matter physics [8, 9].

### B. Correlation in 2D materials

In 2D materials, the charge density can be easily changed by back-gating, enabling correlations to be tuned experimentally in an unprecedented way. In graphene, for example, correlation becomes important when the Fermi energy is close to the Dirac point, and the density of free charges is low [10]. For strongly correlated electronic phases, where electrons are no longer weakly interacting, the DFT treatment no longer provides a valid physical picture. An example of this DFT failure is the description of the electronic states in bilayer graphene twisted at a small angle, forming Moiré superlattices. At specific twist angles, the electronic band dispersion close to the Fermi level is nearly flat on the reciprocal space. When the flat bands are partially filled, the resulting electronic states are highly correlated and can display orbital magnetism, superconductivity, or quantised anomalous Hall effect.[11–15]. Other correlated systems, such as low-density electron gas phases in graphene, are still object of research. Accurate numerical treatment of correlation, such as the random phase approximation (RPA), will be examined in sec. III.

Alternatively, the Reduced Density Matrix Functional Theory (RDMFT), which upgrades DFT by using the reduced density matrix rather than just the spatial density, has proven the ability to deal with strongly correlated systems dominated by static correlations, and in particular to calculate fundamental band gaps of semiconductors/insulators and in transition metal oxides [16, 17] where DFT fails.

### C. Correlation and van der Waals forces

Correlation is also in part responsible for the van der Waals (vdW) bonding [18]. When two-dimensional layers pair up, a charge density redistribution, arising from induced transient dipoles associated with electronic charge fluctuations, generates an attractive force between layers. It is known that local or semi-local exchange-correlation functionals developed for 3D solids yield incorrect vdW binding energies and geometries. However, a correct description of vdW systems can be achieved with low computational overhead by adding a semi-empirical dispersion potential, such a pair-wise force field optimized for several popular DFT functionals, to the conventional Kohn-Sham DFT energy (see Fig. 1) [19–24]. Correlation energy expression to obtain dispersion-corrected functionals to deal with weak interactions can be derived also using the Adiabatic-Connection Fluctuation–Dissipation theorem approach (see for example ref. [25]) within the RPA approximation. These functionals are able to determine the relative thermodynamic stability of different vdW layered superlattices. Conversely, one can argue that the discovery of 2D materials has contributed to this important methodological development.

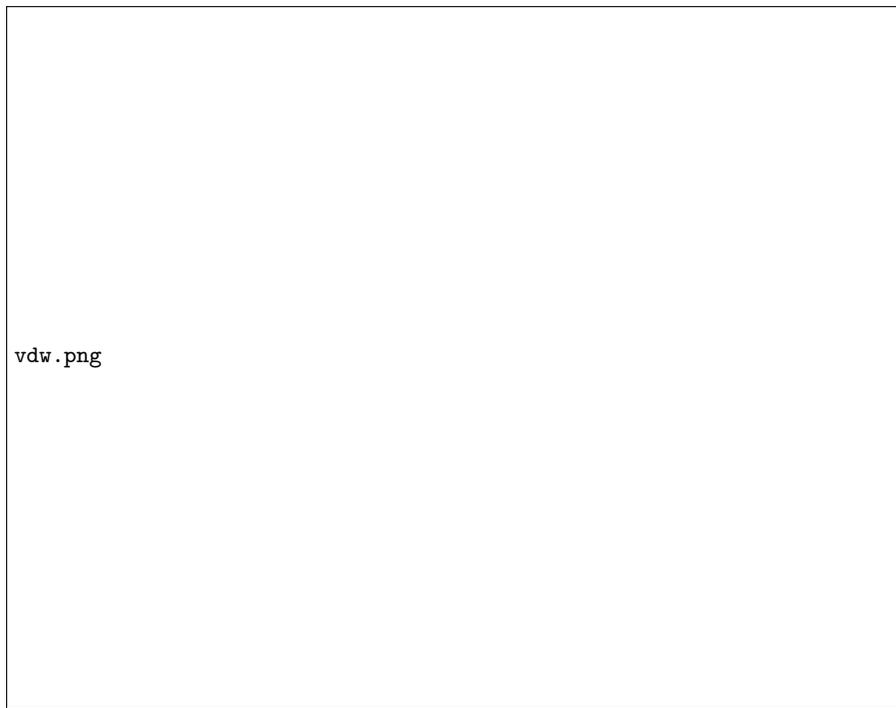


FIG. 1: **Van der Waals functionals.** Comparison of the interlayer distance yield by different levels of treatment of the van der Waals interaction for bulk graphite and boron nitride. Experimental reference values at low temperature are represented by the horizontal lines. Values are from REF.[24]

#### D. Choice of basis set for 2D materials

The majority of DFT codes expand the KS eigenfunctions into a plane wave (PW) basis set [26, 27], owing to the fact that in principle the accuracy can be indefinitely increased by simply increasing the energy cutoff ( $E_{\text{cutoff}}$ ). However, the presence of vacuum between 2D layer replicas and inter-layer spacing raise the computational cost, as the number of PWs increases rapidly at a given  $E_{\text{cutoff}}$ . We will come back to this replica problem in sec. III.

Owing to the hybrid character of 2D materials, the ideal basis set to deal with layered systems, however, is one in which its functions are periodic in-plane while atomic-like along the perpendicular direction [28, 29].

#### E. Electronic structure

The electronic band structure can be calculated (with little formal justification) from the Kohn-Sham (KS) orbital energies  $\epsilon_l(\mathbf{k})$  as a function of the crystal momentum  $\mathbf{k}$ , as well as the Fermi energy from the normalisation constraint. However, we notice that the single electron energies  $\epsilon_l(\mathbf{k})$  describe the dispersion for the auxiliary system obtained by creating an effective potential that is felt by non-interacting electrons. Thus, in metallic systems where e-e interactions dominate, far from the Landau Fermi liquid picture, the one-electron

energies are not a good representation of the many-body electron system. Still, in some instances, they may be used due to their conceptual simplicity.

An immediate application of DFT one-electron energies is the calculation of the bandgap, which can be meaningfully determined from the difference in energies between the lowest unoccupied and the highest occupied KS states [30, 31]. Also this approach is prone to very-well known failures, such as the bandgap underestimation when a local density approximation is used.[4] More accurate methods for reckoning the electronic fundamental band gap and optical spectra of 2D materials will be discussed in Section III.

### III. AB-INITIO MANY-BODY PERTURBATION THEORY IN 2D MATERIALS

#### A. The GW approximation

Excited-state properties and the interpretation of electron spectroscopy experimental measurements in condensed matter physics rely on the concept of quasiparticle (QP), which is represented as a fundamental excitation of bare particle plus its polarization cloud. QPs are not eigenstates of the Hamiltonian and thus acquire finite life-times. In this subsection, we will limit our discussion to particular QPs, the electronic polarons (as originally

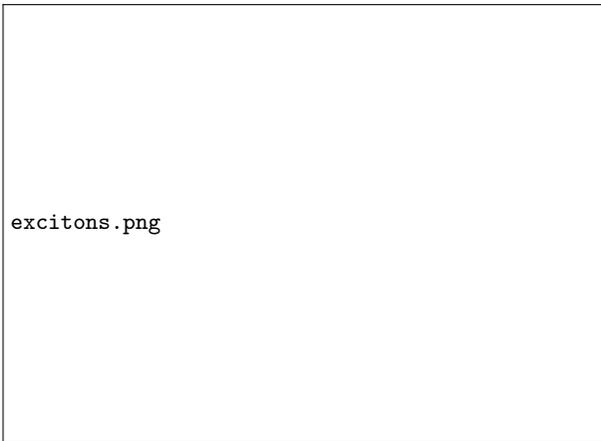


FIG. 2: **Origin of the excitons in the optical absorption spectra of monolayer MoS<sub>2</sub>.** **a**| LDA (dashed blue curve) and GW (solid red curve) band structure. Arrows indicate the optical transitions. **b**| Absorption spectra without (dashed red curve) and with (solid green curve) electron-hole interactions, calculated by solving the BSE. **c**| Same as **b** but using an *ab-initio* broadening based on the electron-phonon interactions. Panels **a-c** are adapted from REF. [32]. Panel **d** is from REF. [33].

defined by L. Hedin [34]), which can be imagined as electrons (or holes) dressed by their electronic clouds.

Within the *ab-initio* many-body perturbation theory (Ai-MBPT) framework for electronic structure calculations, the central quantity is the one-particle Green's function  $G$  (at zero temperature), which is defined as the inverse of the ground state expectation value of the interacting Hamiltonian of the  $N$  electron system ( $|N\rangle$ ). Using this definition, one can write the Dyson equation as follows:

$$G^{-1}(\mathbf{r}_1, \mathbf{r}_2, \omega) \equiv G_0^{-1}(\mathbf{r}_1, \mathbf{r}_2, \omega) - \Sigma(\mathbf{r}_1, \mathbf{r}_2, \omega) \quad (1)$$

where  $G_0^{-1}(\mathbf{r}_1, \mathbf{r}_2, \omega)$  is the inverse of the non-interacting Green's function and  $\Sigma(\mathbf{r}_1, \mathbf{r}_2, \omega)$  is the self-energy.  $\Sigma(\mathbf{r}_1, \mathbf{r}_2, \omega)$  is a non-Hermitian, energy-dependent, and non-local quantity, which “dresses” the bare particle with the whole many-body electron interaction cloud. To describe some important features of Ai-MBPT, it is useful to write  $G$ , through the Lehmann spectral representation [34–36], in terms

of the  $f_s$ , the transition amplitudes from the  $N$ -electron system state  $|N\rangle$  to the excited state  $s$  of the  $N \pm 1$  system  $|N \pm 1; s\rangle$ . In Ai-MBPT, the quantum states  $|N\rangle$  to  $|N \pm 1; s\rangle$  are determined from either the non-interacting DFT or a tight-binding (TB) approximation (see sec. IV A). The QP energies  $E_s^{QP}$  and the amplitudes  $f_s$  are obtained from the homogeneous equation (1):

$$(E_s^{QP} - h - \Sigma(\omega)) f_s(\mathbf{r}) = 0 \quad (2)$$

where the real part of the eigen-energies  $E_s^{QP}$  delivers the QP band structures, while the imaginary part the QP

damping (by means of the imaginary part of  $\Sigma$ ). Both  $f_s$  and  $E_s^{QP}$  are directly related to the spectral function of particles and, therefore to the intrinsic losses in photo-emission spectroscopy (PES) and inverse PES.

GW is the most successful and popular approximation to the self-energy in Ai-MBPT. With respect to DFT calculations, GW improves the agreement with the experimental data of the simulated electronic band structure [35], and reads (the symbol “\*” stands for the convolution product):

$$\Sigma(\mathbf{r}_1, \mathbf{r}_2, \omega) = \frac{i}{2\pi} G_0(\mathbf{r}_1, \mathbf{r}_2, \omega) * W(\mathbf{r}_1, \mathbf{r}_2, \omega) e^{-i\eta\omega} \quad (3)$$

where  $W$  is the screened Coulomb interaction that is related to the *bare* Coulomb potential  $w$  via the dielectric function  $\epsilon$ :

$$W(\mathbf{r}_1, \mathbf{r}_2, \omega) = \int d\mathbf{r}_3 \epsilon^{-1}(\mathbf{r}_1, \mathbf{r}_3, \omega) w(\mathbf{r}_3, \mathbf{r}_2, \omega) \quad (4)$$

$\epsilon(\mathbf{r}_1, \mathbf{r}_3, \omega)$  measures the tendency of a medium to be polarized under the action of an external electromagnetic field, it is related to the energy loss spectrum [37] and energy loss in charge transport Monte Carlo (see sec. IV).

We notice that the GW self-energy is the HF exchange potential in Eq. (3) if the screened Coulomb potential  $W$  is replaced by the bare Coulomb potential  $w$ .

## B. The Bethe–Salpeter equation

Besides one-particle properties, two-particle properties also play a prominent role in the study of excited-state features of 2D materials, namely excitonic effects in absorption spectra. A typical example is the electron-hole (e-h) QP: the exciton. Similarly to QPs theory, the two-body Green's function  $L$  is determined by solving the Bethe–Salpeter equation (BSE):

$$L_{vc,v'c'}^{-1}(\omega) \equiv H_{vc,v'c'}^{\text{BSE}}(\omega) = (E_c^{\text{QP}} - E_v^{\text{QP}}) \delta_{v,v'} \delta_{c,c'} + I_{cv,c'v'}^{\text{eh}}(\omega) \quad (5)$$

where  $v$  and  $c$  are valence and conduction one-particle states,  $H_{vc,v'c'}^{\text{BSE}}(\omega) \equiv \langle vc | \hat{H} | v'c' \rangle$  is the effective two-body Hamiltonian, and  $I_{cv,c'v'}^{\text{eh}}$  is the kernel of this Dyson-type equation, which includes the e-h interactions. In Ai-MBPT, an important assumption for semiconductors and insulators is to approximate the kernel  $I$  with the static screened potential  $I \approx W$ .

In bulk materials, these properties are calculated from the macroscopic dielectric function  $\epsilon_M(\omega)$  which is related to the imaginary part of  $L$  ( $q$  is a reciprocal lattice vector) through:

$$\epsilon_M(\omega) = \lim_{q \rightarrow 0} (1 - v(q) \text{Im} L(q, \omega)) \quad (6)$$

where the long wavelength limit of the interaction Coulomb potential  $v$  must be considered. In 2D materials the macroscopic dielectric function reduces to 1 and,

to determine the optical properties, the longitudinal in-plane polarisability has to be considered [28]:

$$\chi_P(\omega) \approx \lim_{q \rightarrow 0} \frac{1}{q^2} L(q, \omega) \quad (7)$$

Alternatively, one can obtain Eq. (6) by averaging  $W$  over the material rather than the simulation supercell [38].

Figure 2 shows how GW+BSE can be used to interpret the exciton features in MoS<sub>2</sub>, including the optical absorption threshold, exciton binding energy, and spin and momentum-related selection rules.

### C. The screened potential $W$ in 2D materials

The screened potential  $W$  enters in both these approaches and is by far the most difficult to estimate, amongst the many-body terms. It is calculated starting from the non interacting polarization function  $P_0$ , which is determined from the ground (DFT or TB) state energy and wave function. The minimal basis set necessary to obtain accurate results comparable with experiments is usually very large. This issue is increased in quasi-2D materials, where the crystalline periodicity is present only in the planar directions whereas in the  $z$  direction (normal to the plane) the wave functions have a polyatomic molecular character. This hybrid (both crystalline and molecular) behaviour induces, on the plane of the layers, electric field fluctuations that are not screened at large distances: the e-e and e-h interactions are thus much stronger than in 3D materials, producing excitons with notably high binding energy [39–49] and, in presence of defects, extremely stable [48].

By using periodic Ai-MBPT plane-wave codes, quasi-2D materials calculations present the replica issue previously mentioned (see sec. IID). Owing to the ineffective Coulomb interaction screening of the bare  $w$ , the required distance between the replicas can be very large, making calculations unfeasible, as the mesh grid for reciprocal space integration has to be increased. To overcome this problem, the Coulomb interaction is truncated beyond a certain cutoff distance in the  $z$ -direction [38, 50–52]. A slightly different approach [53, 54] consists in replacing  $w$  by a Keldysh-like potential to simulate the in-plane screening of a 2D layer in vacuum,

$$W_{2D}(q) = \frac{2\pi e}{|q|(1 + \alpha_{2D}q)} \quad (8)$$

where  $e$  is the charge and  $q$  is a reciprocal lattice vector in the plane. This potential is often used in connection with TB calculations [55, 56].

Due to their high binding energy, excitons in quasi-2D materials are stable and localized. Qubits [57], single-photon light emitter devices using the self-trapping effects [58], excitonic devices or cavity polaritons [59], and valleytronics [60] are some of the potential applications exploiting these peculiar many-body effects in 2D

materials[39–49].

Finally, 2D materials are often encapsulated or lying over substrates. Several works were devoted to deal with substrate effects on  $W$  [52, 55, 61–63].

### D. Second, third, and higher harmonic generations

The strong optical response of 2D materials to external electromagnetic fields generates peculiar effects also in non-linear regime, giving rise to an optical response at multiples of the exciting frequency  $\omega$ . Graphene and TMD semiconductors show non-trivial topological characteristics [60, 64, 65], which have been investigated with higher harmonic generation calculations [66]. To deal with these physical mechanisms, two different main approaches are developed in the context of Ai-MBPT: the direct integration of the time-dependent macroscopic polarization and the perturbative approach for the non-linear susceptibilities.

The macroscopic polarization  $P(t)$  is the key observable of interest for optical properties. This can be expressed in terms of one-particle reduced density matrix as:

$$\mathbf{P}(t) = e \int \mathbf{r} \hat{\rho}(\mathbf{r}, t) d\mathbf{r} = \frac{e}{A} \sum_{c\nu\mathbf{k}} \mathbf{r}_{c\nu\mathbf{k}} \rho_{c\nu\mathbf{k}}(t), \quad (9)$$

where  $e$  is the charge of the electron, and  $A$  is the 2D crystal area. The time-dependent density matrix is defined as  $\rho_{m\nu\mathbf{k}}(t) \equiv \langle \hat{a}_{m\mathbf{k}}^\dagger(t) \hat{a}_{\nu\mathbf{k}}(t) \rangle$  by the creation (and destruction) operators  $\hat{a}^\dagger$  ( $\hat{a}$ ). In the length gauge [67], the dipole matrix elements  $\mathbf{r}_{m\nu\mathbf{k}} \equiv \langle m\mathbf{k} | \hat{\mathbf{r}} | \nu\mathbf{k} \rangle$  are separated in two components,

the intraband (or Berry Connection [68])  $\mathbf{r}^i$  and the interband dipole operators  $\mathbf{r}^e$  where the indices  $m$  and  $\nu$  are the bands.

In the high harmonic generation optical responses, the e-h interactions are dominant. An ai-MBPT description is provided by the time-dependent (TD) BSE [69]. The TD-BSE is originally derived from the Kadanoff-Baym equation and it can be related to the Lindblad master equation for open quantum systems [70, 71]. If the interaction with the external electric field  $\mathbf{F}$  is written in the length gauge ( $H_{int} = e\mathbf{F} \cdot \mathbf{r}$ ) TD-BSE reads

$$i\hbar \frac{\partial}{\partial t} G_{\mathbf{k}}(t) = \left[ h_{\mathbf{k}} + e\mathbf{F}(t) \cdot \mathbf{r} + \Sigma_{\mathbf{k}}[G_{\mathbf{k}}(t)], G_{\mathbf{k}}(t) \right], \quad (10)$$

where the self-energy  $\Sigma$  is introduced either in the HF approximation or in the static GW self-energy (COHSEX), and  $[\cdot, \cdot]$  is the commutator. In absence of the self-energy (and then, the e-h interactions), the “*semiconductor Bloch equations*” (SBE) is retrieved from the TD-BSE when considering the connection between the Green’s function and the density matrix:  $\mathbf{G}_{n\nu\mathbf{k}}(t) \equiv \mathbf{G}_{n\nu\mathbf{k}}(t, t) = i\rho_{n\nu\mathbf{k}}(t)$ . In the strong-field resonant dynamics and attosecond optoelectronics, the SBE is currently implemented to calculate the band population (diagonal terms) and coherences (the off-diagonal terms),

see subsection III E) [72–74]. Analogous formulas for the density evolution can be retrieved within the time-dependent DFT (TD-DFT) framework, leading to equations analogous to the SBE and TD-BSE (see [66] for an exhaustive review on the topic).

From Eq. (10) the non linear responses such as the second, third, and higher harmonic generations can be estimated with the perturbative derivation of the harmonic generation response functions

$$P = \chi^{(1)}F + \chi^{(2)}FF + \chi^{(3)}FFF + \dots \quad (11)$$

where  $\chi^{(1)}$ ,  $\chi^{(2)}$ ,  $\chi^{(3)}$  are, respectively the macroscopic first, second and, third, order susceptibilities. These high order responses can be analytically derived by expanding the Eq. (10) in terms of one-particle Green's function  $\mathbf{G}_{nm\mathbf{k}}(\omega)$ ,  $\mathbf{G}_{nm\mathbf{k}}(2\omega)$ ,  $\mathbf{G}_{nm\mathbf{k}}(3\omega)$  [55].

Alternatively, macroscopic polarization  $P$  can be obtained through Eq. (9) and with the Green's function time-integration scheme of the eq.10. The linear response (i.e. the BSE (5)) and the higher order generation responses  $\chi^{(i)}$  are retrieved by numerical Fourier transform of  $P(\omega)$  [69, 75].

Ai-MBPT calculations of the optical response of boron nitride show that excitons also dominate the nonlinear optical properties.[55]. Moreover, crystal local field effects, whose importance was already displayed for bulk and surfaces [66], dramatically shape the SHG and THG spectra in MoS<sub>2</sub> and h-BN monolayers [76]. Finally, differently from the linear response regime, the interband and intraband transitions cannot be separated as shown in the SHG and THG calculations in the spectrum of bilayer graphene [77], and in the THG calculations of semiconductor BP [78], MoS<sub>2</sub> and h-BN [55] SLs. Real-time simulations have recently been used to better determine the model used to extract the SHG coefficient from the experimental data, such as in the case of the 2D monochalcogenides GaSe and InSe [79].

### E. Trions, Exciton–polarons, and Biexciton formations

Controlling the optical response of the material by doping the substrate or by gating is a possibility in 2D ma-

terials that has had no parallel in traditional optical materials. Recently, 2D TMDs optical absorption experiments [80, 81] have shown that, in the presence of free carriers, the most prominent excitonic features split into two distinctive peaks. The second peak was initially attributed to trions, i.e. the three-body QP characterised by a bound state of an exciton plus an hole or electron, and later to the dressed excitons, the *exciton-polarons*, that is the many-body generalization of the trion bound and unbound states. It has been theoretically shown that at low doping, the ground state corresponds to the trion and becomes an exciton-polaron at higher doping. [82–84]. From an *ab-initio* point of view, this problem was tackled by extending the Ai-MBPT to include this three-body effective Hamiltonian (e.g. in carbon nanotubes [85, 86]), or to describe the optical spectrum lineshape (e.g. of MoS<sub>2</sub> [87]). In a (two-electrons) plus hole system, *eeh* (the electron and two holes, *hhe*, is analogous) the effective Hamiltonian is approximated as an extension of the BSE (5): the particle-particle interactions are described by the single BSE (an then mediated by the Screened many-body interaction  $W$ ) correlations with the third particle non interacting. The three-body correlation kernel term is disregarded. This Hamiltonian, with a combination of GWA and Configuration Interaction (CI) approaches, has been applied to the case of WS<sub>2</sub> and MoS<sub>2</sub> monolayers [88].

These calculations provide quantitative binding energies of the trion resonances both in a free-standing layer and in a more realistic case with substrate (or encapsulation) that enhances the environmental screening. More importantly, the analysis of transitions has shown the nature of trions [87] (Fig. 5).

Recently in ref.[89], ultrafast pump-probe experiments on monolayer WSe<sub>2</sub> showed the biexcitons signatures and a fine structure in excellent agreement with the theory. The dynamics-controlled truncation theory for biexcitons appear in the THG susceptibility. The biexciton spectrum was modeled with SBE-like equation of motion for the four-particle correlation function:

$$B_{k,k'}^{c'v'cv}(q,t) \equiv \langle \hat{a}_{c'(-k'-q)}^\dagger \hat{a}_{v'k'} \hat{a}_{c(-k)}^\dagger \hat{a}_{v'(k+q)} \rangle (t) - \langle \hat{a}_{c'(-k'-q)}^\dagger \hat{a}_{v'k'} \rangle (t) \langle \hat{a}_{c(-k)}^\dagger \hat{a}_{nv(k+q)} \rangle (t) \quad (12)$$

where the interaction Hamiltonian is described as the extension of trion and two-body BSE Hamiltonian for the 4-particle  $B_{k,k'}^{c'v'cv}$  but in the HF approximation.

### F. Dark and bright exciton formation, photoluminescence and biexciton fine structures in monolayer TMDs.

Besides bright excitons, TMDs exhibit dark excitons that modify the dynamics, the coherence lifetime and,

at last, the photo-luminescence. In a series of articles [90–93], the SBE-like equations for the excitonic density matrices has been extended to include phonon and photon scattering events and describe the exciton dynamics. To summarize, the exciton band structure is calculated from DFT and GW calculations. The Heisenberg equation of motion for the coherent exciton polarization  $P_q(t) \equiv \sum_k \psi_k^* \hat{a}_{c(k+q)}^\dagger \hat{a}_{v(k-q)}(t)$  ( $\psi_k$  the exciton wave-function) is derived. The total Hamiltonian in the SBEs includes the "free" exciton Hamiltonian, incoherent (4-particle) exciton density formation  $N_Q(t) \equiv \sum_{k,k'} \langle \hat{a}_{c(k-\alpha q)}^\dagger \hat{a}_{v(k+\beta q)} \hat{a}_{v(k'+\beta q)}^\dagger \hat{a}_{c(k'-\alpha q)} \rangle(t)$  through the phonon-exciton coupling, and photon-exciton interactions in the low excitation regime. On the same reference, the equation of motion for the incoherent exciton occupation density  $N_Q$  is written including in the Hamiltonian the non-radiative decay of  $P_Q$ , phonon scattering processes (in and out), and the spontaneous photon emission. Between the main results, the theory predicted that a carrier relaxation in TMDs on 50 fs time scale, an order of magnitude faster than in quantum wells whereas the incoherent part of the photoluminescence was estimated to decay on a timescale of few tens of nanoseconds.

#### IV. QUANTUM TRANSPORT

In layered structures, band dispersion and electron transport are both strongly affected by reduced screening and quantum confinement. This results in a wide range of band gaps and charge carrier mobilities (see Fig. 3(a)). On the other hand, highly anisotropic in-plane and out-of-plane electrical properties [102] emerge. For example, in bulk MoS<sub>2</sub>, the in-plane mobility ( $\mu_{x,y}$ ) exceeds the out-of-plane mobility ( $\mu_z$ ) by a factor of  $10^3$  [94], essentially due to the vdW interlayer spacing acting as a tunneling barrier (see Fig. 3(a)). In this section, we consider transport modelling approaches and their applicability in different regimes.

##### A. The tight-binding approach

Tight-Binding (TB) [103] is an approximate quantum-mechanical method to calculate the electronic structure of solids, using a basis set of atomic orbitals  $\phi_i(\mathbf{r})$ , and it is widely used for transport modelling in 2D materials. TB assumes that inside a solid, electrons are tightly bound to the atoms, and that their single particle wave functions  $|\psi_{\mathbf{kn}}\rangle$  in the crystal are quasi-atomic.

The TB scheme has been very successful in modelling graphene, and is easily extendable to other hexagonal 2D materials [95, 104]. In the case of graphene, the Dirac Hamiltonian of chiral massless particles of quantum electrodynamics (QED) in two dimensions can be obtained by considering only first NN interactions between  $p_z$  or-

bitals and by expanding linearly in the momentum the matrix elements of the TB Hamiltonian in the proximity of the  $K$  (or  $K'$ ) point. This results in a  $2 \times 2$  Hamiltonian

$$\mathcal{H}|_K = v_F \hat{\sigma} \cdot \mathbf{p}, \quad (13)$$

where  $\hat{\sigma}$  are the Pauli matrices, and  $v_F = \sqrt{3}\gamma_0 a / (2\hbar)$  is the Fermi velocity. The latter resembles the QED spin Hamiltonian where the Fermi velocity plays the role of the light velocity of massless particles. By including interactions up to third NN  $\pi - \pi^*$  orbitals, it is possible to recover the band asymmetric behaviour far from the Dirac cones.

The TB model is computationally very efficient as it can easily scale up to several million atoms [103]. For example, the TB approach was used to calculate the LDOS in 2D graphene pseudospheres (see Fig. 3(b)) [95, 104] having a few millions carbon atoms with a number of Stone-Wales defects (reproduced in the inset of Fig. 3(c)). The presence of bumps and asymmetries of the bands around the Fermi level, different from graphene's linear dispersion denotes the presence of penta-heptagonal defects related to the negative curvature [95]. TB can also be used to determine the band-structure of twisted bilayer graphene, that shows interesting flat-band effects when the twist angle is small and the respective unit cell very large – too large to be treatable by conventional methods such as DFT (Fig. 4).

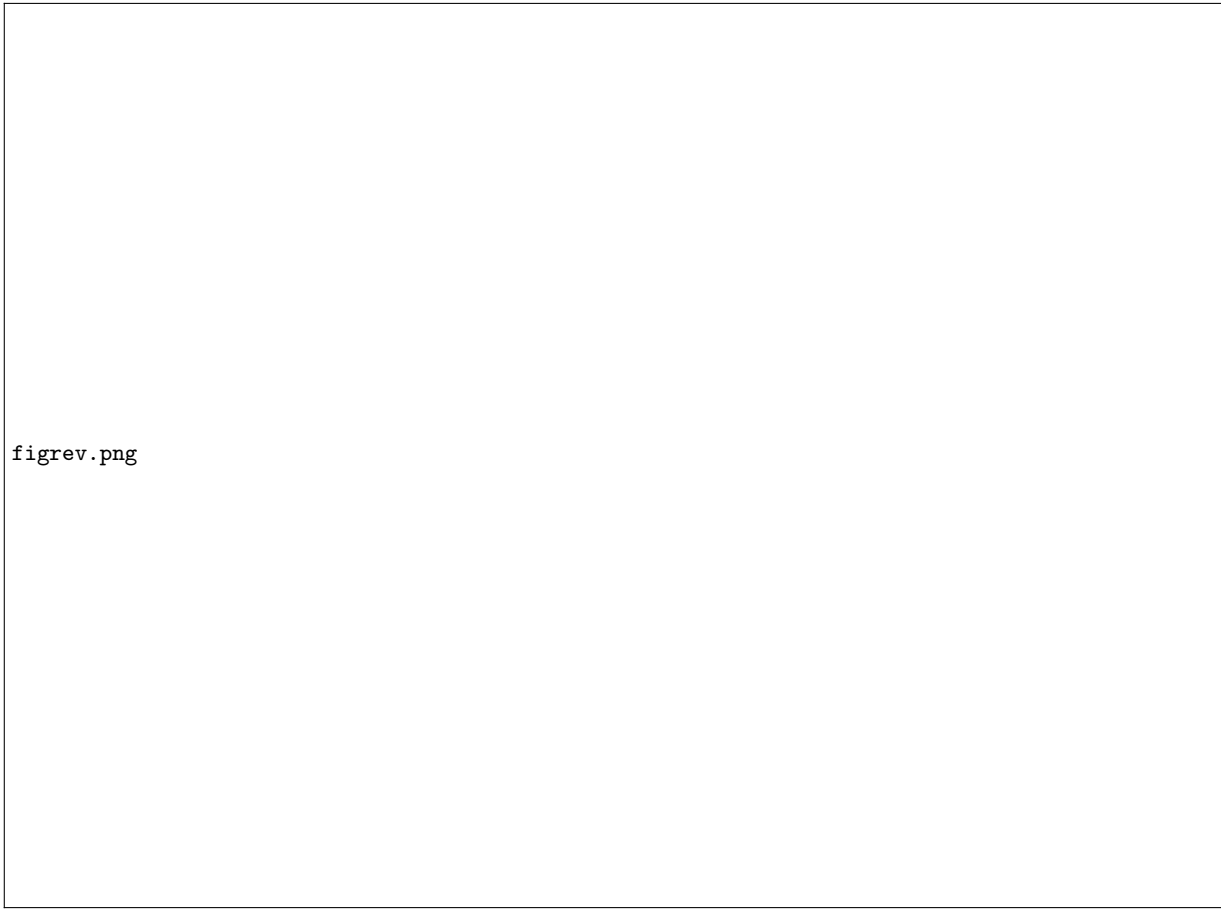
However, TB has limited use in systems where  $d$  electrons contribute substantially to the bands involved in transport, or in general when there is substantial orbital hybridisation.

##### B. Quantum transport: Landauer-Büttiker

The key quantity in the study of charge transport in 2D materials is the coherence length  $l_\phi$ , which measures the length scale of the single-electron wavefunction phase change owing to phase-relaxing processes.  $l_\phi$  determines the crossover between ballistic and diffusive transport regimes. In graphene,  $l_\phi \approx 0.5 \mu\text{m}$ .

In the coherent regime, the standard modelling setup to study mesoscopic transport consists of a system connected to a thermal reservoir by two reflectionless macroscopic contacts that define the temperature and the chemical potential of the incoming electrons (see Fig. 3(d)). Using this layout, one derives the so-called two-probe Landauer-Büttiker (LB) conductivity formula. This formalism can be used both within the quasi-particle Fermi liquid framework and within correlated electrons schemes, when the Coulomb interaction between the flowing electrons breaks down the Landau picture.

In the LB theory, the conduction through the device is represented in terms of scattering processes that the electrons undergo after being injected from the left lead into the device, and before entering the reservoir by crossing



figrev.png

FIG. 3: **Transport and mechanical properties of 2D materials.** **a**| Mobility vs. bandgap of selected 2D materials compared, with those of 3D semiconductors. ML, SL, 3L stand for few-layer, single-layer and tri-layer, respectively, and BP stands for black phosphorus [94]. **b**| Up panel: local density of states (LDOS) symmetry breaking due to curvature effects in a pseudosphere graphene membrane with  $N = 2,615,976$  carbon atoms, evaluated using a TB approach. Bottom: LDOS projected over the two nonequivalent graphene sublattices A and B near the Fermi energy. **c**| Graphene membrane shaped as a Beltrami’s pseudosphere. **d**| Set-up of a typical Landauer-Büttiker (LB) transport simulation. **e**| Logic flow of the LB *ab-initio* approach. **f**| Reflection electron energy loss spectra (REELS) of a highly oriented pyrolytic graphite (HOPG) sample for several primary beam kinetic energies simulated by MC. **g**| Stress–strain curves of liskene, tilene, and flakene along the different strain directions from first-principles simulations. Panels **b-c** are from REF.[95]. Panel **f** is from REF.[96]. Panel **g** is from REF.[97].

the right lead. Within the LB scheme the conductance reads:

$$I = \frac{2e}{h} \int 4\mathbf{Tr}[\Gamma_L G_D^{r\dagger} \Gamma_R G_D^r] [f(E - \mu_L) - f(E - \mu_R)] dE \quad (14)$$

where  $T(E) = 4\mathbf{Tr}[\Gamma_L G_D^{r\dagger} \Gamma_R G_D^r]$  is the lead-to-lead transmission probability of an electron of energy  $E$ , the integral is over all available energies, and the factor 2 counts the spin multiplicity. The intrinsic energy linewidths  $\Gamma_{L/R} = \frac{i}{2}[\Sigma_{L/R}^r - \Sigma_{L/R}^{r\dagger}]$  of the left and right leads account for the finite lifetime of the electrons moving from the central region, where the conductance is described in terms of the retarded Green’s function (rGF) of the device ( $G_D^r$ ), to the leads.

The main tasks of the LB approach consist thus in the accurate evaluation of the self-energies associated with the left and right electrodes, and of the

Green’s function (GF) of the central region (the device). These tasks can be accomplished via two different computational schemes: (i) GF evaluation recursive methods, similar to the techniques used in connection to TB Hamiltonians;[105–107]. (ii) *ab-initio* approaches[108, 109]. A schematic logic flow of the steps involved in the *ab initio* simulation of the LB approach to transport is reported in Fig. 3(e). Figure 6 illustrates an *ab-initio* calculation of device voltage-current characteristics based on the LB approach.

### C. Quantum transport: Kubo approach

A second, widely used quantum mechanical approach for coherent, noninteracting electrons is based on the Kubo formalism [111]. The Kubo approach is a broadly

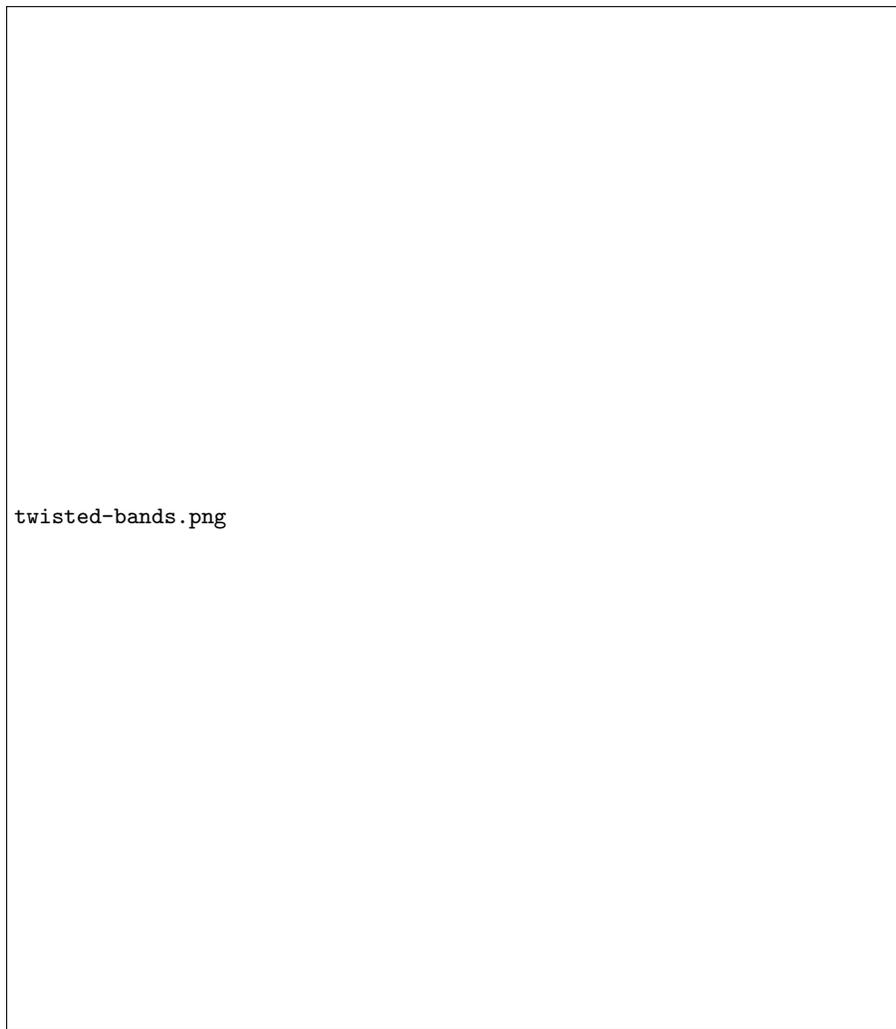


FIG. 4: **Tight-binding bandstructure of twisted bilayer graphene.** **a**] Moiré lattice in real space and **b**] its reciprocal space. Primitive cells for the angle ( $\theta$ ) of interest have thousands of atoms and are often too large to be modelled by DFT. **c-e**] Scanning tunneling microscopy images at different angles ( $\theta_{g-\bar{g}}$ ) and related periodicity  $\lambda_{g-\bar{g}}$ . The images are for twisted bilayer graphene over BN, but the BN is not visible. Band structures for fully relaxed twisted bilayer graphene obtained with a tight-binding model, for angles slightly above ( $1.08^\circ$ ), very close ( $1.02^\circ$ ), and slightly below ( $0.93^\circ$ ) the ‘magic’ angle at which the bands close to the Fermi level become flat. Panels **a-b** are from REF. [98]. Panels **c-e** are from REF. [99]. Panels **f-h** are from Ref. [100].

applicable technique, based on the linear response of a material to an externally applied electric field and on the fluctuation–dissipation theorem. In quantum transport [112–114], this theorem relates the conductivity  $\sigma(\omega)$ , ie. the dissipative out-of-equilibrium response at frequency  $\omega$  (which can be derived from the current density  $\mathcal{J}(\omega) = \sigma(\omega)E(\omega)$ , where  $E(\omega)$  is the applied electric field), with the correlation function of the charge carrier velocities, which measures the fluctuations that the system undergoes by applying e.g. an external (weak) electric field. In 2D materials, these fluctuations correspond to electronic transitions between states of the system at equilibrium induced by an oscillating field  $E(\omega) = E_0 \cos(\omega t)$ , which are connected to the total

power absorbed per unit time and volume

$$\mathcal{P} = \mathcal{J}\dot{E} = \sigma\langle E\dot{E} \rangle = \sigma E_0^2/2. \quad (15)$$

Using this theorem, at first-order perturbation theory in the electric field one obtains the Kubo conductivity [111]:

$$\sigma(\omega) = \frac{\pi\hbar e^2}{\Omega} \sum_{m,n} |\langle m|v_{pl}|n \rangle|^2 \delta(E_m - E_n - \hbar\omega) [f(E_n) - f(E_m)] \quad (16)$$

where  $\Omega$  is the sample volume,  $E_m, E_n$  are the energies of the levels  $m, n$ ,  $f(E_{n,m})$  is the Fermi–Dirac distribution,  $e$  is the electric charge, and  $v_{pl}$  is the projection of the velocity operator  $\mathbf{v}$  on the axial direction within the 2D plane.

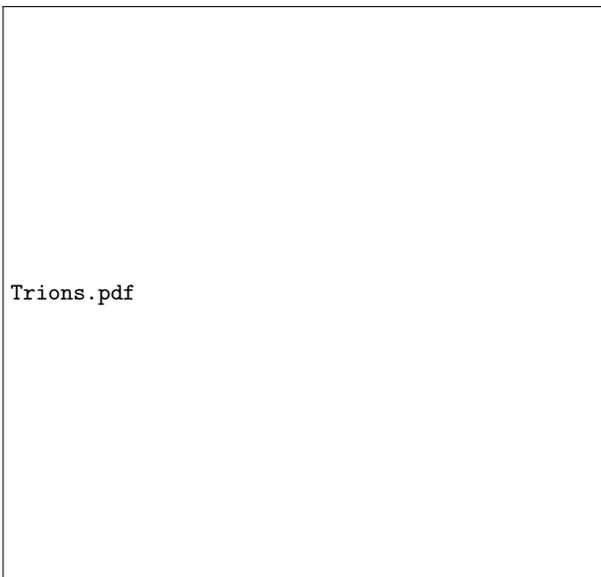


FIG. 5: **MoS<sub>2</sub> monolayer spectrum from Ai-MBP** showing excitonic spectrum (red) and trion contribution (blue). **a|** Negative trions and **b|** positive trions exhibit resonant states (close to the A and B exciton). The A<sup>-</sup> trion is split into three separate peaks, labeled A<sub>(1,2,3)</sub><sup>(-)</sup>. From REF. [101].



FIG. 6: **Multi-scale simulation of a MoS<sub>2</sub> transistor device.** The simulation of a ‘planar barristor’ is based on DFT, Green’s function formalism and Landauer-Büttiker formula. **a|** Transistor scheme in single gate (SG) and double gate (DG) configuration. **b|** Transfer characteristics in linear/semilogarithmic scale of the DG planar barristor, and of the SG planar barristors with different oxide thicknesses.  $I_{DS}$ ,  $V_G$  and  $V_{DS}$  stand for the drain-source current, gate voltage and drain-source voltage, respectively. From REF. [110]

The calculation of the Kubo conductivity is computationally very expensive owing to the numbers of orbitals that must be included in the simulation. Efficient real-space implementations have been proposed in Refs. [95, 113, 115]. The Kubo approach has been applied for example to simulate transport characteristics of several carbon-based materials [112, 116–121] (Fig. 3d,e).

Finally, the Kubo and the LB approaches can be reconciled and are actually equivalent in some given conditions, most notably if the quantum transmission at the system/electrode interface is perfect. The Kubo approach is better suited to investigate the transport properties of disordered materials, characterized by localization phenomena in the low-temperature limit. For example, it has been used to compute the low-energy dependence of the electronic conductivity of pristine and disordered graphene [122]. It can be directly compared to experimental four-points transport measurements. At variance, the LB transport formalism is better suited to study charge transport through a system connected to external electrodes. It has a direct connection with two-point transport measurements.

#### D. Semiclassical approaches: Boltzmann Transport Equation

In diffusive regime, where electrons are characterised by lifetimes  $\tau_D$  longer than the decoherence time  $l_\phi$ , particles undergo a sequence of phase-breaking scattering events, which can be dealt with at semiclassical level.

A typical example of such sequential process is the Coulomb blockade [123], where electrons are resonantly tunnelled one by one at only some values of the gate voltage and blocked otherwise. Conductance shows a set of sharp peaks corresponding to the resonant energies, which can be tuned by changing the gate voltages. This principle can be used in single-electron transistors [124].

Typically, the sequential regime is modelled by rate equations, such as the following Boltzmann transport equation (BTE):

$$\left[ \frac{\partial}{\partial t} + \mathbf{v}_k \cdot \nabla_{\mathbf{r}} + \mathbf{F} \cdot \nabla_{\mathbf{k}} \right] f_k(\mathbf{r}, t) = \frac{\partial f_k(\mathbf{r}, t)}{\partial t} \Big|_{\text{coll}} \quad (17)$$

in which the quantum particle dynamics, under the external force-field  $\mathbf{F}$ , is described via a distribution function or particle density  $f_k(\mathbf{r}, t)$ . The term in the right hand side of Eq. 17 accounts for particle-particle collisions that drive the system toward equilibrium.

Typically the solution of the BTE [115] is found within the Relaxation Time Approximation (RTA), which assumes that

$$\frac{\partial f_k(\mathbf{r}, t)}{\partial t} \Big|_{\text{coll}} = -\frac{g_k}{\tau_k}, \quad (18)$$

where  $g_k = f_k - f_k^{eq}$  represents the variation of the distribution function  $f_k(\mathbf{r}, t)$  from the equilibrium Fermi-Dirac

distribution  $f_k^{eq}(\mathbf{r}, t)$  at temperature  $T$ . The relaxation time  $\tau_k$  is the time that the system takes to relax to  $f_k^{eq}(\mathbf{r}, t)$  after the external force-field is switched off.

The time-scale  $\tau_k$  is typically assumed to be inversely proportional to the probability of scattering from the momentum state  $|k'\rangle$  to  $|k\rangle$ , as given by Fermi's golden rule. Finally, the calculation of the Boltzmann conductivity  $\sigma$  within RTA is derived from the current density as:

$$\sigma = \frac{-e^2}{2\pi} \int k dk \left( \frac{\partial f_k^{eq}(\mathbf{r}, \mathbf{t})}{\partial \epsilon_k} \right) \tau_k v_k^2 \quad (19)$$

where  $\epsilon_k$  can be obtained via TB model simulations. Note that the BTE is a semiclassical equation, neglecting quantum interference between particles.

### E. Semiclassical approaches: Monte-Carlo

A semiclassical Monte Carlo (MC) statistical method can be used to evaluate the carrier transport when the De Broglie wavelength of the electrons or holes is significantly smaller than their mean separation. This method considers electrons or holes as point-like particles, whose motion within the sample is defined by classical trajectories [125, 126]. However, the quantum nature of the charged particles is accounted for in the calculation of the elastic and inelastic scattering cross sections. The MC approach deals with several different possible scattering mechanisms: (i) elastic scattering with atomic nuclei, producing angular deviation of the electron/hole trajectories; (ii) inelastic e-e interaction leading to electron energy loss, secondary electron generation and angular deviation; (iii) electron-phonon interaction, typically introduced in a semi-empirical fashion at fixed energy loss; and (iv) trapping phenomena that end the trajectory (e.g. polaron quasi-particle excitations).

The electron path is generally assumed to be described by a Poisson-like law, so the step length ( $\Delta s$ ) between two subsequent collisions is given by:

$$\Delta s = -l_{\text{tot}} \ln(r), \quad (20)$$

where  $l_{\text{tot}} = \frac{1}{N\sigma}$  is the total mean free path and  $r$  is a uniformly distributed random number in the range  $[0 : 1]$ . The electron transport in the sample is simulated by generating a statistically significant number of trajectories, usually in excess of  $10^9$ , to achieve a low noise-to-signal ratio.

Using this MC approach it is possible to simulate the anisotropic features of electron transport in layered materials. An example is the calculation of the plasmonic spectrum in highly oriented pyrolytic graphite (HOPG)[96] (see Fig. 3(f)).

The e-ph interaction matrix elements, whose square values are directly related to the carrier-phonon scattering rate via Fermi's golden rule, can be evaluated using a DFT/DFPT framework. Here density functional perturbation theory [127] (DFPT) is used to obtain the phononic dispersion relations, based on the

DFT electronic structure. This approach has been used e.g. to estimate the temperature-dependent intrinsic scattering rates as a function of electron/hole energy in layered semiconductors. For example, such calculations have been used to clarify the reason for the lower carrier mobilities measured in transition metal dichalcogenides (TMDCs), compared to graphene, and the regimes where the mobility is defect-limited [128] or phonon-limited[129]. However, the multivalley nature of the band structure requires the inclusion of spin-dependent functionals to account for the spin-orbit band splitting, which is strong in TMDs and can affect charge transport, particularly in the valence band. Additionally, many-body approaches beyond DFT should be used for an accurate assessment of the band energies, which can have a severe bandgap underestimation in DFT.

## V. MECHANICAL PROPERTIES

While the optical, electrical, and transport properties of 2D materials are extensively investigated for their potential application in microelectronics, many of the current commercial applications of 2D materials rely on their mechanical strength. In addition, they are also expected to play a pivotal role in flexible electronics [130], and therefore their mechanical properties are of major interest. Theoretical approaches for studying mechanical properties can be categorised into three classes: (1) continuum mechanics (CM), e.g. based on finite elements (FEM) methods, and peridynamics [131]; (2) atomistic simulation based on classical molecular dynamics (MD); (3) ab-initio simulations based on DFT or TB.

DFT yields accurate elastic constants, especially those corresponding to in-plane deformations, as covalent bond energies are quantitatively more accurate than vdW energies. DFT is typically applied to defect-free materials with a limited number of atoms in the unit cell, lower than 100. The elastic constants can be calculated from the total energy at 0 K, for selected deformations. For example, Fig. 3(g) illustrates the simulation, using DFT, of the stress-strain characteristics of several 2D carbon allotropes with density lower than graphene[97].

Nevertheless, the mechanical properties of real materials are often dominated by defects, such as dislocations, and vary considerably from those of the perfect crystals. Thus, models at larger scale are needed. One alternative are semi-empirical TB calculations,[132] which were for example used to simulate armors based on carbon or hybrid layers [131]. In that study, a size-scale transition from the nano- to the microscale in the impact behaviour was found by adopting a multiscale approach based on FEM and CM models.

For larger computational systems, in a space-time scale of  $\approx 1\mu\text{m}$  and  $\approx 1\text{ ns}$ , classical MD simulations are mainly used. In classical MD simulation, electrons are not explicitly included, and the interatomic potentials between atoms in the systems are typically modelled by two-

body or reactive semi-empirical force-fields [133], such as condensed-phase optimized molecular potentials (COMPASS) [134], reactive empirical bond order (REBO) potentials [135], or adaptive intermolecular reactive empirical bond order (AIREBO) potentials [136]. These proved effective in the analysis of the mechanical behaviors of several carbon-based 2D materials, e.g. strained graphene [137–142], and carbon-based foams [143, 144]. However, parameterised potentials are not readily available for all element combinations and types of bonding, and substantial effort may be required to set up and test a classical simulation for a new material. Today, machine learning, trained on DFT data, is also used to generate this empirical potential [145].

## VI. OUTLOOK

The revolutionary advances that 2D materials have known over the last ten years have been greatly supported by computational modelling. Conversely, the development of computational methods is often driven by the need to explain new experimental results. A major motivation that drives experimental and theoretical efforts is to find new materials and devices able to achieve superior information density and higher energy efficiency with respect to conventional electronics, or to support flexible electronics. In parallel however, many groups investigating 2D materials have been driven by the possibility of studying new physical phenomena. This in turn brings new questions to be answered by theoretical and computational means.

For example, the description of effects induced by correlation in confined systems remains a challenge, owing to the difficulty in describing both the stronger electron-electron interaction and the more ineffective screening of external electromagnetic fields with respect to the 3D counterpart. Computational modelling is still hampered by the widespread use of basis sets adopting 3D periodic boundary conditions, which are not naturally adapted to 2D systems. This approach leads to an unnecessary computational expenditure and, specially in GW, to reduced accuracy. Furthermore, pristine 2D materials are unstable against the creation of flexural phonons and magnons (for ferromagnetic systems), as a result of the Mermin-Wagner-Hohenberg theorem. It is not surprising that these collective excitations are still challenging to model in 2D, owing to the difficulty in accounting for substrate dampening effects, or the numerical instability resulting from the lack of dampening in free layers.

Further methodological advances are also desirable in the computational treatment of the excitonic phenomena that have no counterpart in 3D. This is mainly due to the lack of dielectric screening outside the plane, which stabilises excitons, trions, biexcitons, etc. Additionally, in vdW structures, the possibility of forming quasi-particles localised in different layers, such as inter-layer excitons, opens up intriguing possibilities. For ex-

ample, in heterostructures with layers stacked at a finite twist-angle, leading to Moiré superlattices, it is possible to choose both the momentum displacement between the electron and hole bands and the confining potential. The computational description of the resulting Moiré excitons, including new selection rules [146, 147] and trapped/delocalised phases [148], is an extremely active area of research.

First-principles approaches able to treat electronic excitations, based on TD-BSE and TD-DFT, demonstrated their potential to interpret experimental outcomes. Nevertheless, *ab-initio* TD-BSE is computationally expensive and TD-DFT suffers from a kernel that takes into account accurately the excitonic effects. In this regard, the computational development is focusing on numerical approaches that are able to accelerate the calculations.

The *ab-initio* description of exciton-phonon polaron QPs, characterised by Coulomb correlations renormalized by lattice dynamics via polaronic effects, is still in its infancy. In particular, to achieve a complete theoretical treatment to predict the full excitonic dispersion in 2D materials is a complex challenge, as one would need to include in one unified framework several microscopic ingredients, such as spin-orbit coupling, exchange interactions, many-body correlations, and polaronic effects. Non-equilibrium exciton dynamics and its effects in the optical and electronic properties of 2D materials, such as the carrier-density dependent optical spectra, are very challenging for first principles calculations but can be tackled using density matrix theory.[149–151]

Twisted Moiré multilayers, as well as other 2D systems, such as FeSe monolayers, have recently revealed the emergence of many interesting electronic phases, including orbital magnetism, superconductivity, or quantised anomalous Hall effect [11–15, 152]. However, an adequate computational modelling of highly correlated electronic phases in 2D materials is still lacking [153, 154], particularly in presence of external magnetic fields, such as those routinely applied to probe these phases in experiments.

Ferromagnetic systems are also an emerging area within 2D materials research. Although there is at present no doubt that 2D ferromagnetic materials are stable, there is still lack of information on the role of boundary conditions, substrate, etc. in stabilising magnetism. Similar remarks apply to 2D ferroelectrics: for example, it is not completely understood the critical thickness dependence of ferroelectric polarization, as well as the relevant experimental conditions. Since ferromagnetism and ferroelectricity are very dependent on defects and boundary conditions, we believe that computational studies will be paramount to unravel these questions. Other important emerging areas that we must mention are related to the modelling of magnetic excitations, such as skyrmions.

We point out also the need for developing computational methods to calculate macroscopic observables that are scalable and computationally effective in terms of memory requirements and CPU usage, notably for modelling realistic systems. There is still ample room for de-

velopment of first-principles based multiscale approaches to calculate macroscopic observables and to link the properties of 2D materials to the measurable electrical response of real devices, such as carrier mobilities, thermal conductivity, ionic conductivity, spin lifetime, etc. While computer simulations and experimental measurements have quantified the intrinsic carrier mobility of quite a few 2D materials, its assessment in presence of substrates and external fields, at real-scale geometries, is still challenging for computer simulations. Further, many systems of technological interest are not crystalline but amorphous (such as graphene oxide), or are molecular 2D layers (such as 2D water).

Finally, emerging areas of computational research in 2D materials modelling aim to machine learning models and inverse design[1, 2, 155–157]. Machine learning is

being used e.g. to revolutionise the fitting of classical inter-atomic potentials or other approximate models by replacing the considerable human effort with an artificial neural network [158, 159]. This may change classical modelling approaches and make them promptly available in the area of application.

## VII. ACKNOWLEDGEMENTS

AC and AHCN were supported by the National Research Foundation, Prime Minister Office, Singapore, under its Medium Sized Centre Programme and CRP award “Novel 2D materials with tailored properties: beyond graphene” (Grant number R-144-000-295-281).

- 
- [1] Zunger, A. Inverse design in search of materials with target functionalities. *Nature Reviews Chemistry* **2**, 1–16 (2018).
- [2] Ren, Z. *et al.* Inverse design of crystals using generalized invertible crystallographic representation. *arXiv preprint arXiv:2005.07609* (2020).
- [3] Lejaeghere, K. *et al.* Reproducibility in density functional theory calculations of solids. *Science* **351** (2016).
- [4] Hohenberg, P. & Kohn, W. Inhomogeneous electron gas. *Phys. Rev.* **136**, B864–B871 (1964).
- [5] Gillan, M. J. The virtual matter laboratory. *Contemporary Physics* **38**, 115–130 (1997).
- [6] Wigner, E. & Seitz, F. On the constitution of metallic sodium. *Phys. Rev.* **43**, 804–810 (1933).
- [7] Helbig, N., Tokatly, I. & Rubio, A. Exact Kohn–Sham potential of strongly correlated finite systems. *The Journal of chemical physics* **131**, 224105 (2009).
- [8] Gross, E. K. U., Petersilka, M. & Grabo, T. Conventional quantum-chemical correlation energy vs. density functional correlation energy. In Laird, B. B., Ross, R. B. & Ziegler, T. (eds.) *Chemical Applications of Density Functional Theory*, vol. 629, 42 (American Chemical Society, Washington, D.C., 1993).
- [9] Gritsenko, O. V., Schipper, P. R. T. & Baerends, E. J. Exchange and correlation energy in density functional theory: Comparison of accurate density functional theory quantities with traditional hartree–fock based ones and generalized gradient approximations for the molecules  $\text{Li}_2$ ,  $\text{N}_2$ ,  $\text{F}_2$ . *The Journal of Chemical Physics* **107**, 5007–5015 (1997).
- [10] Kotov, V. N., Uchoa, B., Pereira, V. M., Guinea, F. & Neto, A. C. Electron-electron interactions in graphene: Current status and perspectives. *Reviews of Modern Physics* **84**, 1067 (2012).
- [11] Cao, Y. *et al.* Correlated insulator behaviour at half-filling in magic-angle graphene superlattices. *Nature* **556**, 80–84 (2018).
- [12] Cao, Y. *et al.* Unconventional superconductivity in magic-angle graphene superlattices. *Nature* **556**, 43–50 (2018).
- [13] Yankowitz, M. *et al.* Tuning superconductivity in twisted bilayer graphene. *Science* **363**, 1059–1064 (2019).
- [14] Lu, X. *et al.* Superconductors, orbital magnets and correlated states in magic-angle bilayer graphene. *Nature* **574**, 653–657 (2019).
- [15] Serlin, M. *et al.* Intrinsic quantized anomalous hall effect in a moiré heterostructure. *Science* **367**, 900–903 (2020).
- [16] Sharma, S., Dewhurst, J. K., Lathiotakis, N. N. & Gross, E. K. U. Reduced density matrix functional for many-electron systems. *Phys. Rev. B* **78**, 201103 (2008).
- [17] Sharma, S., Dewhurst, J. K., Shallcross, S. & Gross, E. K. U. Spectral density and metal-insulator phase transition in mott insulators within reduced density matrix functional theory. *Phys. Rev. Lett.* **110**, 116403 (2013).
- [18] Kawai, S. *et al.* Van der Waals interactions and the limits of isolated atom models at interfaces. *Nature communications* **7**, 11559 (2016).
- [19] Klimeš, J. & Michaelides, A. Perspective: Advances and challenges in treating van der Waals dispersion forces in density functional theory. *The Journal of chemical physics* **137**, 120901 (2012).
- [20] Grimme, S. Density functional theory with london dispersion corrections. *WIREs Computational Molecular Science* **1**, 211–228 (2011).
- [21] Johnson, E. R., Mackie, I. D. & DiLabio, G. A. Dispersion interactions in density-functional theory. *Journal of Physical Organic Chemistry* **22**, 1127–1135 (2009).
- [22] Burns, L. A., Mayagoitia, A. V., Sumpter, B. G. & Sherrill, C. D. Density-functional approaches to noncovalent interactions: A comparison of dispersion corrections (dft-d), exchange-hole dipole moment (xhm) theory, and specialized functionals. *The Journal of Chemical Physics* **134**, 084107 (2011).
- [23] Björkman, T., Gulans, A., Krashennnikov, A. V. & Nieminen, R. M. Van der Waals bonding in layered compounds from advanced density-functional first-principles calculations. *Physical review letters* **108**, 235502 (2012).
- [24] Lebedeva, I. V., Lebedev, A. V., Popov, A. M. & Knizhnik, A. A. Comparison of performance of van der Waals-corrected exchange-correlation functionals for interlayer interaction in graphene and hexagonal boron nitride.

- Computational Materials Science* **128**, 45–58 (2017).
- [25] Patrick, C. E. & Thygesen, K. S. Adiabatic-connection fluctuation-dissipation dft for the structural properties of solids—the renormalized alda and electron gas kernels. *The Journal of Chemical Physics* **143**, 102802 (2015).
- [26] Giannozzi, P. *et al.* Advanced capabilities for materials modelling with quantum espresso. *Journal of Physics: Condensed Matter* **29**, 465901 (2017).
- [27] Kresse, G. & Furthmüller, J. Efficient iterative schemes for ab initio total-energy calculations using a plane-wave basis set. *Physical review B* **54**, 11169 (1996).
- [28] Trevisanutto, P. E. & Vignale, G. Ab initio electronic structure of quasi-two-dimensional materials: A “native” gaussian–plane wave approach. *The Journal of chemical physics* **144**, 204122 (2016).
- [29] Do, V. N., Le, H. A. & Vu, V. T. Real-space and plane-wave hybrid method for electronic structure calculations for two-dimensional materials. *Phys. Rev. B* **95**, 165130 (2017).
- [30] Seidl, A., Görling, A., Vogl, P., Majewski, J. A. & Levy, M. Generalized Kohn-Sham schemes and the band-gap problem. *Phys. Rev. B* **53**, 3764–3774 (1996).
- [31] Perdew, J. P. *et al.* Understanding band gaps of solids in generalized Kohn–Sham theory. *Proceedings of the national academy of sciences* **114**, 2801–2806 (2017).
- [32] Qiu, D. Y., da Jornada, F. H. & Louie, S. G. Optical spectrum of mos<sub>2</sub>: Many-body effects and diversity of exciton states. *Phys. Rev. Lett.* **111**, 216805 (2013).
- [33] Mak, K. F., Lee, C., Hone, J., Shan, J. & Heinz, T. F. Atomically thin mos<sub>2</sub>: A new direct-gap semiconductor. *Phys. Rev. Lett.* **105**, 136805 (2010).
- [34] Hedin, L. Electron correlation: Keeping close to an orbital description. *International Journal of Quantum Chemistry* **56**, 445–452 (1995).
- [35] Onida, G., Reining, L. & Rubio, A. Electronic excitations: density-functional versus many-body green’s-function approaches. *Rev. Mod. Phys.* **74**, 601–659 (2002).
- [36] Hedin, L. & Lundqvist, S. Effects of electron-electron and electron-phonon interactions on the one-electron states of solids. In Seitz, F., Turnbull, D. & Ehrenreich, H. (eds.) *Solid State Physics*, vol. 23, 1 – 181 (Academic Press, 1970).
- [37] Nazarov, V. U., Silkin, V. M. & Krasovskii, E. E. Probing mesoscopic crystals with electrons: One-step simultaneous inelastic and elastic scattering theory. *Phys. Rev. B* **96**, 235414 (2017).
- [38] Hüser, F., Olsen, T. & Thygesen, K. S. How dielectric screening in two-dimensional crystals affects the convergence of excited-state calculations: Monolayer mos<sub>2</sub>. *Phys. Rev. B* **88**, 245309 (2013).
- [39] Qiu, D. Y., da Jornada, F. H. & Louie, S. G. Optical spectrum of mos<sub>2</sub>: Many-body effects and diversity of exciton states. *Phys. Rev. Lett.* **111**, 216805 (2013).
- [40] Ugeda, M. M. *et al.* Giant bandgap renormalization and excitonic effects in a monolayer transition metal dichalcogenide semiconductor. *Nature Materials* **13**, 1091–1095 (2014).
- [41] Tran, V., Soklaski, R., Liang, Y. & Yang, L. Layer-controlled band gap and anisotropic excitons in few-layer black phosphorus. *Phys. Rev. B* **89**, 235319 (2014).
- [42] Bradley, A. J. *et al.* Probing the role of interlayer coupling and coulomb interactions on electronic structure in few-layer mos<sub>2</sub> nanostructures. *Nano Letters* **15**, 2594–2599 (2015).
- [43] Liu, K. *et al.* Evolution of interlayer coupling in twisted molybdenum disulfide bilayers. *Nature Communications* **5**, 4966 (2014).
- [44] Andersen, K., Latini, S. & Thygesen, K. S. Dielectric genome of van der Waals heterostructures. *Nano Letters* **15**, 4616–4621 (2015).
- [45] Gomes, L. C., Trevisanutto, P. E., Carvalho, A., Rodin, A. S. & Castro Neto, A. H. Strongly bound mott-wannier excitons in ges and gese monolayers. *Phys. Rev. B* **94**, 155428 (2016).
- [46] Guo, L. *et al.* Exchange-driven intravalley mixing of excitons in monolayer transition metal dichalcogenides. *Nature Physics* **15**, 228–232 (2019).
- [47] Arora, A. *et al.* Interlayer excitons in a bulk van der Waals semiconductor. *Nature Communications* **8**, 639 (2017).
- [48] Zheng, Y. J. *et al.* Point defects and localized excitons in 2d wse<sub>2</sub>. *ACS Nano* **13**, 6050–6059 (2019).
- [49] Bernardi, M., Palumbo, M. & Grossman, J. C. Extraordinary sunlight absorption and one nanometer thick photovoltaics using two-dimensional monolayer materials. *Nano Letters* **13**, 3664–3670 (2013).
- [50] Rozzi, C. A., Varsano, D., Marini, A., Gross, E. K. U. & Rubio, A. Exact coulomb cutoff technique for supercell calculations. *Phys. Rev. B* **73**, 205119 (2006).
- [51] Castro, A., Räsänen, E. & Rozzi, C. A. Exact coulomb cutoff technique for supercell calculations in two dimensions. *Phys. Rev. B* **80**, 033102 (2009).
- [52] Latini, S., Olsen, T. & Thygesen, K. S. Excitons in van der Waals heterostructures: The important role of dielectric screening. *Phys. Rev. B* **92**, 245123 (2015).
- [53] Cudazzo, P., Attaccalite, C., Tokatly, I. V. & Rubio, A. Strong charge-transfer excitonic effects and the bose-einstein exciton condensate in graphane. *Phys. Rev. Lett.* **104**, 226804 (2010).
- [54] Cudazzo, P., Tokatly, I. V. & Rubio, A. Dielectric screening in two-dimensional insulators: Implications for excitonic and impurity states in graphane. *Phys. Rev. B* **84**, 085406 (2011).
- [55] Pedersen, T. G. Intraband effects in excitonic second-harmonic generation. *Phys. Rev. B* **92**, 235432 (2015).
- [56] Ridolfi, E., Lewenkopf, C. H. & Pereira, V. M. Excitonic structure of the optical conductivity in mos<sub>2</sub> monolayers. *Phys. Rev. B* **97**, 205409 (2018).
- [57] Maragkou, M. The dark exciton as a qubit. *Nature Materials* **14**, 260–260 (2015).
- [58] Aharonovich, I., Englund, D. & Toth, M. Solid-state single-photon emitters. *Nature Photonics* **10**, 631–641 (2016).
- [59] Unuchek, D. *et al.* Room-temperature electrical control of exciton flux in a van der Waals heterostructure. *Nature* **560**, 340–344 (2018).
- [60] Schaibley, J. R. *et al.* Valleytronics in 2d materials. *Nature Reviews Materials* **1**, 16055 (2016).
- [61] Trolle, M. L., Pedersen, T. G. & Véliard, V. Model dielectric function for 2d semiconductors including substrate screening. *Scientific Reports* **7**, 39844 (2017).
- [62] Rodin, A. S., Carvalho, A. & Castro Neto, A. H. Excitons in anisotropic two-dimensional semiconducting crystals. *Phys. Rev. B* **90**, 075429 (2014).
- [63] Rohlfing, M. Electronic excitations from a perturbative LDA + *gdw* approach. *Phys. Rev. B* **82**, 205127 (2010).

- [64] Xu, X., Yao, W., Xiao, D. & Heinz, T. F. Spin and pseudospins in layered transition metal dichalcogenides. *Nat. Phys.* **10**, 343–350 (2014).
- [65] Liu, H. *et al.* High-harmonic generation from an atomically thin semiconductor. *Nat. Phys.* **13**, 262 (2016).
- [66] Luppi, E. & Vénard, V. A review of recent theoretical studies in nonlinear crystals: towards the design of new materials. *Semiconductor Science and Technology* **31**, 123002 (2016).
- [67] Aversa, C. & Sipe, J. E. Nonlinear optical susceptibilities of semiconductors: Results with a length-gauge analysis. *Phys. Rev. B* **52**, 14636–14645 (1995).
- [68] Resta, R. Macroscopic polarization in crystalline dielectrics: the geometric phase approach. *Rev. Mod. Phys.* **66**, 899–915 (1994).
- [69] Attaccalite, C., Grüning, M. & Marini, A. Real-time approach to the optical properties of solids and nanostructures: Time-dependent bethe-salpeter equation. *Phys. Rev. B* **84**, 245110 (2011).
- [70] Breuer, H.-P. & Petruccione, F. *The Theory of Open Quantum Systems* (Oxford University Press, 2007).
- [71] Wismer, M. S. & Yakovlev, V. S. Gauge-independent decoherence models for solids in external fields. *Phys. Rev. B* **97**, 144302 (2018).
- [72] Heide, C. *et al.* Attosecond-fast internal photoemission. *Nature Photonics* **14**, 219–222 (2020).
- [73] Sederberg, S. *et al.* Attosecond optoelectronic field measurement in solids. *Nature Communications* **11**, 430 (2020).
- [74] Wismer, M. S., Kruchinin, S. Y., Ciappina, M., Stockman, M. I. & Yakovlev, V. S. Strong-field resonant dynamics in semiconductors. *Phys. Rev. Lett.* **116**, 197401 (2016).
- [75] Takimoto, Y., Vila, F. D. & Rehr, J. J. Real-time time-dependent density functional theory approach for frequency-dependent nonlinear optical response in photonic molecules. *The Journal of Chemical Physics* **127**, 154114 (2007).
- [76] Grüning, M. & Attaccalite, C. Second harmonic generation in *h*-bn and *mos*<sub>2</sub> monolayers: Role of electron-hole interaction. *Phys. Rev. B* **89**, 081102(R) (2014).
- [77] Hipolito, F., Taghizadeh, A. & Pedersen, T. G. Nonlinear optical response of doped monolayer and bilayer graphene: Length gauge tight-binding model. *Phys. Rev. B* **98**, 205420 (2018).
- [78] Hipolito, F. & Pedersen, T. G. Optical third harmonic generation in black phosphorus. *Phys. Rev. B* **97**, 035431 (2018).
- [79] Attaccalite, C., Palumbo, M., Cannuccia, E. & Grüning, M. Second-harmonic generation in single-layer monochalcogenides: A response from first-principles real-time simulations. *Phys. Rev. Materials* **3**, 074003 (2019).
- [80] Sidler, M. *et al.* Fermi polaron-polaritons in charge-tunable atomically thin semiconductors. *Nature Physics* **13**, 255–261 (2017).
- [81] Mak, K. F. *et al.* Tightly bound trions in monolayer *mos*<sub>2</sub>. *Nature Materials* **12**, 207–211 (2013).
- [82] Efimkin, D. K. & MacDonald, A. H. Many-body theory of trion absorption features in two-dimensional semiconductors. *Phys. Rev. B* **95**, 035417 (2017).
- [83] Tan, L. B. *et al.* Interacting polaron-polaritons. *Phys. Rev. X* **10**, 021011 (2020).
- [84] Chang, Y.-C., Shiau, S.-Y. & Combescot, M. Crossover from trion-hole complex to exciton-polaron in *n*-doped two-dimensional semiconductor quantum wells. *Phys. Rev. B* **98**, 235203 (2018).
- [85] Deilmann, T., Drüppel, M. & Rohlfing, M. Three-particle correlation from a many-body perspective: Trions in a carbon nanotube. *Phys. Rev. Lett.* **116**, 196804 (2016).
- [86] Deilmann, T., Drüppel, M. & Rohlfing, M. Erratum: Three-particle correlation from a many-body perspective: Trions in a carbon nanotube [phys. rev. lett. 116, 196804 (2016)]. *Phys. Rev. Lett.* **123**, 259902 (2019).
- [87] Drüppel, M., Deilmann, T., Krüger, P. & Rohlfing, M. Diversity of trion states and substrate effects in the optical properties of an *mos*<sub>2</sub> monolayer. *Nature Communications* **8**, 2117 (2017).
- [88] Torche, A. & Bester, G. First-principles many-body theory for charged and neutral excitations: Trion fine structure splitting in transition metal dichalcogenides. *Phys. Rev. B* **100**, 201403 (2019).
- [89] Steinhoff, A. *et al.* Biexciton fine structure in monolayer transition metal dichalcogenides. *Nature Physics* **14**, 1199–1204 (2018).
- [90] Steinhoff, A. *et al.* Nonequilibrium carrier dynamics in transition metal dichalcogenide semiconductors. *2D Materials* **3**, 031006 (2016).
- [91] Selig, M. *et al.* Dark and bright exciton formation, thermalization, and photoluminescence in monolayer transition metal dichalcogenides. *2D Materials* **5**, 035017 (2018).
- [92] Brem, S. *et al.* Phonon-assisted photoluminescence from indirect excitons in monolayers of transition-metal dichalcogenides. *Nano Letters* **20**, 2849–2856 (2020).
- [93] Steinhoff, A., Rösner, M., Jahnke, F., Wehling, T. O. & Gies, C. Influence of excited carriers on the optical and electronic properties of *mos*<sub>2</sub>. *Nano Letters* **14**, 3743–3748 (2014). PMID: 24956358.
- [94] Sangwan, V. K. & Hersam, M. C. Electronic transport in two-dimensional materials. *Annual Review of Physical Chemistry* **69**, 299–325 (2018).
- [95] Morresi, T. *et al.* Exploring event horizons and hawking radiation through deformed graphene membranes. *2D Materials* (2020).
- [96] Azzolini, M. *et al.* Anisotropic approach for simulating electron transport in layered materials: computational and experimental study of highly oriented pyrolytic graphite. *The Journal of Physical Chemistry C* **122**, 10159–10166 (2018).
- [97] Morresi, T. *et al.* Structural, electronic and mechanical properties of all-sp<sup>2</sup> carbon allotropes with density lower than graphene. *Carbon* **159**, 512–526 (2020).
- [98] Jorio, A. & Cançado, L. G. Raman spectroscopy of twisted bilayer graphene. *Solid State Communications* **175–176**, 3 – 12 (2013). Special Issue: Graphene V: Recent Advances in Studies of Graphene and Graphene analogues.
- [99] Wong, D. *et al.* Local spectroscopy of moiré-induced electronic structure in gate-tunable twisted bilayer graphene. *Phys. Rev. B* **92**, 155409 (2015).
- [100] Carr, S., Fang, S., Zhu, Z. & Kaxiras, E. Exact continuum model for low-energy electronic states of twisted bilayer graphene. *Physical Review Research* **1**, 013001 (2019).
- [101] Drüppel, M., Deilmann, T., Krüger, P. & Rohlfing, M. Diversity of trion states and substrate effects in the op-

- tical properties of an mos<sub>2</sub> monolayer. *Nature Communications* **8**, 2017 (2017).
- [102] Zhang, G. & Zhang, Y.-W. Thermal properties of two-dimensional materials. *Chinese Physics B* **26**, 034401 (2017).
- [103] Lherbier, A. *et al.* Transport properties of graphene containing structural defects. *Phys. Rev. B* **86**, 075402 (2012).
- [104] Taioli, S., Gabbriellini, R., Simonucci, S., Pugno, N. M. & Iorio, A. Lobachevsky crystallography made real through carbon pseudospheres. *Journal of Physics: Condensed Matter* **28**, 13LT01 (2016).
- [105] Guinea, F., Tejedor, C., Flores, F. & Louis, E. Effective two-dimensional hamiltonian at surfaces. *Phys. Rev. B* **28**, 4397–4402 (1983).
- [106] Sancho, M. P. L., Sancho, J. M. L., Sancho, J. M. L. & Rubio, J. Highly convergent schemes for the calculation of bulk and surface green functions. *Journal of Physics F: Metal Physics* **15**, 851–858 (1985).
- [107] Pastawski, H. M., Weisz, J. F. & Albornoz, S. Matrix continued-fraction calculation of localization length. *Phys. Rev. B* **28**, 6896–6903 (1983).
- [108] Sanvito, S., Lambert, C. J., Jefferson, J. H. & Bratkovsky, A. M. General green’s-function formalism for transport calculations with spd hamiltonians and giant magnetoresistance in co- and ni-based magnetic multilayers. *Phys. Rev. B* **59**, 11936–11948 (1999).
- [109] Rocha, A. R. *Theoretical and computational aspects of electronic transport at the nanoscale*. Ph.D. thesis, University of Dublin, Trinity College (2007). PhD thesis.
- [110] Marian, D. *et al.* Transistor concepts based on lateral heterostructures of metallic and semiconducting phases of mos<sub>2</sub>. *Phys. Rev. Applied* **8**, 054047 (2017).
- [111] Kubo, R. The fluctuation-dissipation theorem. *Reports on Progress in Physics* **29**, 255–284 (1966).
- [112] Lherbier, A., Biel, B., Niquet, Y.-M. & Roche, S. Transport length scales in disordered graphene-based materials: Strong localization regimes and dimensionality effects. *Phys. Rev. Lett.* **100**, 036803 (2008).
- [113] Roche, S. & Mayou, D. Conductivity of quasiperiodic systems: A numerical study. *Phys. Rev. Lett.* **79**, 2518–2521 (1997).
- [114] Triozon, F. *Diffusion quantique et conductivité dans les système apériodique*. Ph.D. thesis, Université Joseph Fourier (2002). PhD thesis.
- [115] Torres, L., Roche, S. & Charlier, J. *Introduction to Graphene-Based Nanomaterials: From Electronic Structure to Quantum Transport* (Cambridge University Press, 2014).
- [116] Ishii, H., Triozon, F., Kobayashi, N., Hirose, K. & Roche, S. Charge transport in carbon nanotubes based materials: a kubo–greenwood computational approach. *Comptes Rendus Physique* **10**, 283 – 296 (2009). Carbon nanotube electronics.
- [117] Latil, S., Roche, S. & Charlier, J.-C. Electronic transport in carbon nanotubes with random coverage of physisorbed molecules. *Nano Letters* **5**, 2216–2219 (2005).
- [118] Lherbier, A., Blase, X., Niquet, Y.-M., Triozon, F. m. c. & Roche, S. Charge transport in chemically doped 2d graphene. *Phys. Rev. Lett.* **101**, 036808 (2008).
- [119] Roche, S. Quantum transport by means of O(*n*) real-space methods. *Phys. Rev. B* **59**, 2284–2291 (1999).
- [120] Roche, S. & Saito, R. Magnetoresistance of carbon nanotubes: From molecular to mesoscopic fingerprints. *Phys. Rev. Lett.* **87**, 246803 (2001).
- [121] Roche, S., Jiang, J., Triozon, F. m. c. & Saito, R. Quantum dephasing in carbon nanotubes due to electron-phonon coupling. *Phys. Rev. Lett.* **95**, 076803 (2005).
- [122] Nomura, K. & MacDonald, A. H. Quantum transport of massless dirac fermions. *Phys. Rev. Lett.* **98**, 076602 (2007).
- [123] Beenakker, C. W. J. Theory of coulomb-blockade oscillations in the conductance of a quantum dot. *Phys. Rev. B* **44**, 1646–1656 (1991).
- [124] Fu, Y., Dutta, A., Willander, M. & Oda, S. Carrier conduction in a si-nanocrystal-based single-electron transistor-i. effect of gate bias. *Superlattices and Microstructures* **28**, 177 – 187 (2000).
- [125] Taioli, S., Simonucci, S., Calliari, L. & Dapor, M. Electron spectroscopies and inelastic processes in nanoclusters and solids: Theory and experiment. *Physics reports* **493**, 237–319 (2010).
- [126] Dapor, M. *Transport of Energetic Electrons in Solids*. Springer Tracts in Modern Physics (Springer International Publishing, 2020).
- [127] Baroni, S., de Gironcoli, S., Dal Corso, A. & Giannozzi, P. Phonons and related crystal properties from density-functional perturbation theory. *Rev. Mod. Phys.* **73**, 515–562 (2001).
- [128] Kaasbjerg, K., Low, T. & Jauho, A.-P. Electron and hole transport in disordered monolayer mos<sub>2</sub>: Atomic vacancy induced short-range and coulomb disorder scattering. *Phys. Rev. B* **100**, 115409 (2019).
- [129] Jin, Z., Li, X., Mullen, J. T. & Kim, K. W. Intrinsic transport properties of electrons and holes in monolayer transition-metal dichalcogenides. *Phys. Rev. B* **90**, 045422 (2014).
- [130] Zhan, H., Guo, D. & Xie, G. Two-dimensional layered materials: from mechanical and coupling properties towards applications in electronics. *Nanoscale* **11**, 13181–13212 (2019).
- [131] Signetti, S., Taioli, S. & Pugno, N. M. 2d material armors showing superior impact strength of few layers. *ACS Applied Materials & Interfaces* **9**, 40820–40830 (2017).
- [132] Hourahine, B. *et al.* Dftb+, a software package for efficient approximate density functional theory based atomistic simulations. *The Journal of Chemical Physics* **152**, 124101 (2020).
- [133] Senftle, T. P. *et al.* The reaxff reactive force-field: development, applications and future directions. *npj Computational Materials* 15011 (2016).
- [134] Sun, H. Compass: An ab initio force-field optimized for condensed-phase applicationsoverview with details on alkane and benzene compounds. *The Journal of Physical Chemistry B* **102**, 7338–7364 (1998).
- [135] Brenner, D. W. Relationship between the embedded-atom method and tersoff potentials. *Phys. Rev. Lett.* **63**, 1022–1022 (1989).
- [136] Stuart, S. J., Tutein, A. B. & Harrison, J. A. A reactive potential for hydrocarbons with intermolecular interactions. *The Journal of Chemical Physics* **112**, 6472–6486 (2000).
- [137] Zhao, H., Min, K. & Aluru, N. R. Size and chirality dependent elastic properties of graphene nanoribbons under uniaxial tension. *Nano Letters* **9**, 3012–3015 (2009).
- [138] Sakhaee-Pour, A. Elastic properties of single-layered graphene sheet. *Solid State Communications* **149**, 91 –

- 95 (2009).
- [139] Sakhaee-Pour, A. Elastic buckling of single-layered graphene sheet. *Computational Materials Science* **45**, 266–270 (2009).
- [140] Zhang, Y. Y., Pei, Q. X. & Wang, C. M. Mechanical properties of graphynes under tension: A molecular dynamics study. *Applied Physics Letters* **101**, 081909 (2012).
- [141] Zheng, Y., Wei, N., Fan, Z., Xu, L. & Huang, Z. Mechanical properties of grafold: a demonstration of strengthened graphene. *Nanotechnology* **22**, 405701 (2011).
- [142] Neek-Amal, M. & Peeters, F. M. Nanoindentation of a circular sheet of bilayer graphene. *Phys. Rev. B* **81**, 235421 (2010).
- [143] Pedrielli, A., Taioli, S., Garberoglio, G. & Pugno, N. Mechanical and thermal properties of graphene random nanofoams via molecular dynamics simulations. *Carbon* **132**, 766–775 (2018).
- [144] Pedrielli, A., Taioli, S., Garberoglio, G. & Pugno, N. M. Designing graphene based nanofoams with nonlinear auxetic and anisotropic mechanical properties under tension or compression. *Carbon* **111**, 796–806 (2017).
- [145] van der Giessen, E. *et al.* Roadmap on multiscale materials modeling. *Modelling and Simulation in Materials Science and Engineering* **28**, 043001 (2020).
- [146] Wu, F., Lovorn, T. & MacDonald, A. Theory of optical absorption by interlayer excitons in transition metal dichalcogenide heterobilayers. *Physical Review B* **97**, 035306 (2018).
- [147] Yu, H., Wang, Y., Tong, Q., Xu, X. & Yao, W. Anomalous light cones and valley optical selection rules of interlayer excitons in twisted heterobilayers. *Physical review letters* **115**, 187002 (2015).
- [148] Brem, S., Linderälv, C., Erhart, P. & Malic, E. Tunable phases of moiré excitons in van der Waals heterostructures. *Nano Letters* (2020).
- [149] Steinhoff, A., Rosner, M., Jahnke, F., Wehling, T. O. & Gies, C. Influence of excited carriers on the optical and electronic properties of  $\text{mos}_2$ . *Nano letters* **14**, 3743–3748 (2014).
- [150] Steinhoff, A. *et al.* Biexciton fine structure in monolayer transition metal dichalcogenides. *Nature Physics* **14**, 1199–1204 (2018).
- [151] Selig, M. *et al.* Dark and bright exciton formation, thermalization, and photoluminescence in monolayer transition metal dichalcogenides. *2D Materials* **5**, 035017 (2018).
- [152] Kreisel, A., Hirschfeld, P. J. & Andersen, B. M. On the remarkable superconductivity of fese and its close cousins. *Symmetry* **12**, 1402 (2020).
- [153] Kotov, V. N., Uchoa, B., Pereira, V. M., Guinea, F. & Castro Neto, A. H. Electron-electron interactions in graphene: Current status and perspectives. *Rev. Mod. Phys.* **84**, 1067–1125 (2012).
- [154] Tang, H.-K. *et al.* The role of electron-electron interactions in two-dimensional dirac fermions. *Science* **361**, 570–574 (2018).
- [155] Mounet, N. *et al.* Two-dimensional materials from high-throughput computational exfoliation of experimentally known compounds. *Nature Nanotechnology* **13**, 246–252 (2018).
- [156] Rasmussen, F. & Thygesen, K. Computational 2d materials database: Electronic structure of transition-metal dichalcogenides and oxides. *The Journal of Physical Chemistry Part C* **119**, 13169–13183 (2015).
- [157] Zhou, J. *et al.* 2dmatpedia, an open computational database of two-dimensional materials from top-down and bottom-up approaches. *Scientific Data* **6**, 86 (2019).
- [158] Mortazavi, B. *et al.* Machine-learning interatomic potentials enable first-principles multiscale modeling of lattice thermal conductivity in graphene/borophene heterostructures. *Materials Horizons* (2020).
- [159] Vasudevan, R. K. *et al.* Investigating phase transitions from local crystallographic analysis based on machine learning of atomic environments. *arXiv preprint arXiv:2006.10001* (2020).